

PAPER

Real-time and high-transmission middle-infrared optical imaging system based on a pixel-wise metasurface micro-polarization array

To cite this article: Lifeng Ma *et al* 2023 *Chinese Phys. B* **32** 084201

View the [article online](#) for updates and enhancements.

You may also like

- [Dust Reverberation Mapping in Distant Quasars from Optical and Mid-infrared Imaging Surveys](#)
Qian Yang, Yue Shen, Xin Liu et al.
- [Multichannel spectrometers in animals](#)
Thomas W Cronin, Missael Garcia and Viktor Gruev
- [A Revised View of the Linear Polarization in the Subparsec Core of M87 at 7 mm](#)
Jongho Park, Keiichi Asada, Masanori Nakamura et al.

Real-time and high-transmission middle-infrared optical imaging system based on a pixel-wise metasurface micro-polarization array

Lifeng Ma(马丽凤)^{1,†}, Shan Du(杜杉)^{1,†}, Jun Chang(常军)^{1,‡}, Weilin Chen(陈蔚霖)¹, Chuhan Wu(武楚晗)², Xinxin Shi(石鑫鑫)¹, Yi Huang(黄翼)¹, Yue Zhong(钟乐)¹, and Quanquan Mu(穆全全)³

¹School of Optics and Photonics, Beijing Institute of Technology, Beijing 100081, China

²Information Science Academy, China Electronics Technology Group Corporation, Beijing 100098, China

³State Key Laboratory of Applied Optics, China Changchun Institute of Optics, Fine Mechanics and Physics, Changchun 130033, China

(Received 9 June 2022; revised manuscript received 19 October 2022; accepted manuscript online 9 December 2022)

Real-time polarization medium-wave infrared (MIR) optical imaging systems enable the acquisition of infrared and polarization information for a target. At present, real-time polarization MIR devices face the following problems: poor real-time performance, low transmission and high requirements for fabrication and integration. Herein, we aim to improve the performance of real-time polarization imaging systems in the MIR waveband and solve the above-mentioned defects. Therefore, we propose a MIR polarization imaging system to achieve real-time polarization-modulated imaging with high transmission as well as improved performance based on a pixel-wise metasurface micro-polarization array (PMMPA). The PMMPA element comprises several linear polarization (LP) filters with different polarization angles. The optimization results demonstrate that the transmittance of the center field of view for the LP filters is up to 77% at a wavelength of 4.0 μm and an extinction ratio of 88 dB. In addition, a near-diffraction-limited real-time MIR imaging optical system is designed with a field of view of 5° and an F -number of 2. The simulation results show that an MIR polarization imaging system with excellent real-time performance and high transmission is achieved by using the optimized PMMPA element. Therefore, the method is compatible with the available optical system design technologies and provides a way to realize real-time polarization imaging in MIR wavebands.

Keywords: real-time, middle infrared optical imaging system, metasurface, polarization array

PACS: 42.15.-I, 42.25.Ja, 42.15.Eq, 42.79.-e

DOI: 10.1088/1674-1056/aca25

1. Introduction

Polarization imaging reveals optical anisotropic properties, which is important for identifying pathological tissues,^[1] characterizing the structures of materials^[2] and detecting and recognizing targets on a complex background.^[3] Infrared polarization imaging detection has developed rapidly over the past few decades.^[4–6] Compared with conventional infrared imaging technology, infrared polarization detection can acquire deeper information about an object, such as surface shape, roughness, optical activity of the materials and chemical properties. Conventional infrared polarization imaging methods include simultaneous polarization imaging and time-sharing polarization imaging. Division-of-aperture (DOAP) and division-of-focal-plane (DOFP) polarization imaging stand out from the multitude of available infrared polarization imaging systems.^[7–11] Both DOAP and DOFP polarization imaging systems can synchronize polarization data at every frame. Thus, a real-time polarization imaging method can acquire polarization information for a real-time moving object.

A DOFP detector is often used in visible light polarization systems,^[12,13] but is rarely used in medium-wave infrared (MIR) polarization imaging systems. Most MIR polarization

devices^[14] achieve polarization information for the target with the help of DOAP and polarization rotation. Liu^[15] designed a polarization and multispectral imaging system with DOAP to realize the polarization intensity imaging of different spectra in the target. Zhao *et al.*^[16] captured images by rotating a spectral filter and a polarimetric filter in a multispectral polarization system. However, the rotation-polarizer system had poor real-time performance and could easily cause optical axis deviation. DOAP infrared polarization systems have some drawbacks, such as low resolution and difficulty in real-time imaging. To overcome the difficulties in designing and fabricating a DOFP array detector for use in the MIR waveband, in this study the pixel-wise metasurface micro-polarization array (PMMPA) element is placed in the intermediate image plane to realize real-time MIR polarization imaging. In addition, the proposed system can acquire multi-polarization angles of the emergent light without the use of a DOFP detector. The size of the PMMPA element is the same as that of the MIR detector. Meanwhile, the size of a single array of the PMMPA is equivalent to that of a commercial MIR detector pixel.

The metasurface is a class of novel ultrathin optical elements that exhibit excellent ability to simultaneously and independently modulate the nature of light, such as phase, polarization, and amplitude. In addition, with the assistance of

[†]These authors contributed equally to this work.

[‡]Corresponding author. E-mail: optics.chang@126.com

massive design freedoms^[17–20] as well as versatile modulation mechanisms provided by the metasurface,^[21–25] many applications for realizing polarization detection and imaging have been demonstrated. Capasso^[26] proposed the theory of matrix Fourier optics. Moreover, they demonstrated a diffraction grating whose diffraction orders behave as polarizers with controlled polarization responses to realize compact full-Stokes imaging. Chen^[27] designed and fabricated a multifocal axicon meta-lens to achieve parallel polarization illumination to improve the quality of polarization imaging. Yao^[28] presented a bifocal meta-lens that can realize a switchable multiplane by changing the polarization state of the incident light. The polarization dependence was formulated and processed by arranging polysilicon nanobeam unit elements. However, the combination of metasurface and polarization is used in the visible to near-infrared spectrum. Meanwhile, the imaging quality and modulation accuracy of the polarization imaging system can be further improved by integrating the metasurface and the optical system design.

In this work, we demonstrate a MIR polarization imaging system to achieve real-time polarization-modulated imaging based on a metasurface. The optimized PMMPA element can improve the transmission efficiency and extinction ratio of transmitted light. By changing the height, duty cycle and period length of the nanofin on the substrate of the polarization array, different polarization transmittances are analyzed. Furthermore, a MIR polarization optical system is designed based on optical imaging principles. The proposed system comprises an objective lens group and a relay image group. To ensure the vertical incidence on PMMPA elements of different field lights, the image-side dual telecentric system and object-side dual telecentric system are designed for the objective lens group and relay image group. In addition, the simulation results show that a PMMPA element placed on an intermediate image plane can realize real-time multi-angle polarized MIR imaging.

The remainder of this paper is organized as follows. In Section 2, the elements of the PMMPA are designed and optimized. The transmittance and extinction ratio of the PMMPA elements with different structures are analyzed. The structure of the PMMPA element is determined. In Section 3, the MIR optical system is calculated and optimized. The quality of the imaging is analyzed and the PMMPA element and MIR system are combined. In Section 4, after simulation verification, the PMMPA element placed in the middle of the image plane can achieve multi-angle polarization imaging simultaneously.

2. Pixel-wise micro-polarization metasurface array element design

A schematic diagram of the PMMPA real-time MIR optical imaging system, which includes the MIR object-lens,

PMMPA, MIR relay lens, and MIR detector, is shown in Fig. 1(a). The incident light first enters the MIR objective system. The PMMPA element is placed in the image plane of the objective lens, which modulates the polarization properties of the emergent light. The light passing through the PMMPA element is turned into linearly polarized light at different polarization angles. Finally, the modulated linearly polarized light passes through the MIR relay lens group and reaches the detector. High-efficiency real-time polarization images with different polarization angles are obtained. The PMMPA element and its components are shown in Fig. 1(b). The key element of this device is the optimized metasurface polarization array, which modulates the polarization properties of the incident light. The PMMPA element comprises multiple pixels, and each pixel has one spatially distributed linear polarization (LP) filter, as shown in Fig. 1(b). The LP filter groups are nanowire gratings oriented in four different directions to transmit linearly polarized light, whose electric field direction vectors are oriented at 0° , 45° , 90° and 135° with respect to the x -axis. As shown in Fig. 1(c), the LP filter group transmits the TM-polarized light with an electric field direction perpendicular to the grating grooves, while blocking the transmission of TE-polarized light with the electric field direction parallel to the grating grooves.

The intensities of the different polarization components in incident light passing through the optimized polarized filters can be described as I_{0° , I_{45° , I_{90° and I_{135° , respectively. When incident light crosses the PMMPA element, the LP filter at different positions modulates the incident light accordingly, and the detector can capture the intensities of the different polarization states of the light. Subsequently, by combining the left-handed circularly polarized and the right-handed circularly polarized components, the full Stokes parameters can be retrieved by analyzing and processing the polarization components. The derivation process is as follows.

The full-Stokes vectors S have four parameters S_0 , S_1 , S_2 and S_3 , which are defined as

$$S_0 = I_{0^\circ} + I_{90^\circ}, \quad (1)$$

$$S_1 = I_{0^\circ} - I_{90^\circ}, \quad (2)$$

$$S_2 = I_{45^\circ} - I_{135^\circ}, \quad (3)$$

$$S_3 = I_R - I_L. \quad (4)$$

Here I_{0° , I_{45° , I_{90° and I_{135° represent the intensities of the LP components along 0° , 45° , 90° and 135° with respect to the x -axis, respectively. I_R and I_L are the intensities of the right-handed circularly polarized light and left-handed circularly polarized light, respectively. By combining the transmission coefficients of the PMMPA element, which is defined as t_{xx} in this study, the intensities for the four polarization angles can be obtained.

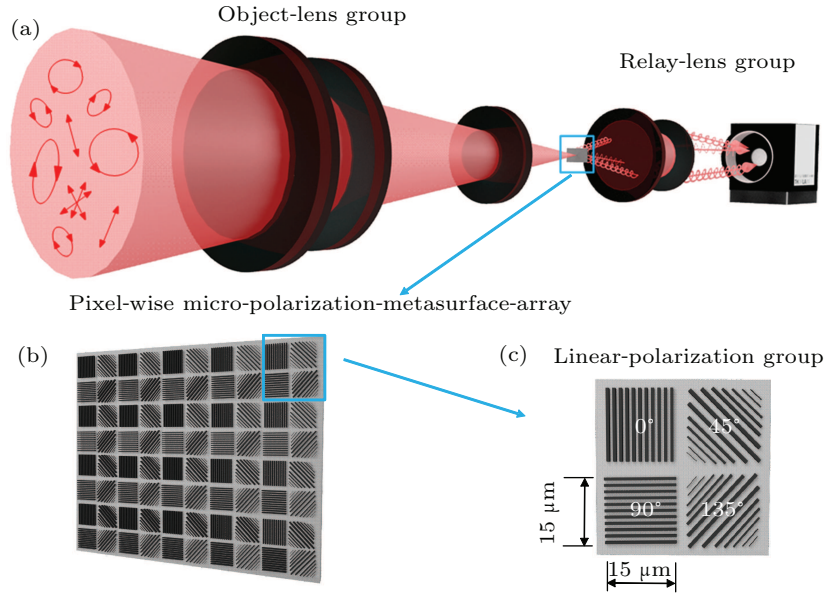


Fig. 1. Schematic diagram of pixel-wise micro-polarization metasurface array real-time MIR optical imaging system. (a) Schematic diagram of the MIR polarized optical system with a PMMPA element. (b) Schematic diagram of a micro-polarization metasurface array element that produces linearly polarized light at four polarization angles. (c) Pixel-level linear polarization group comprising four linear polarizers in the polarization direction.

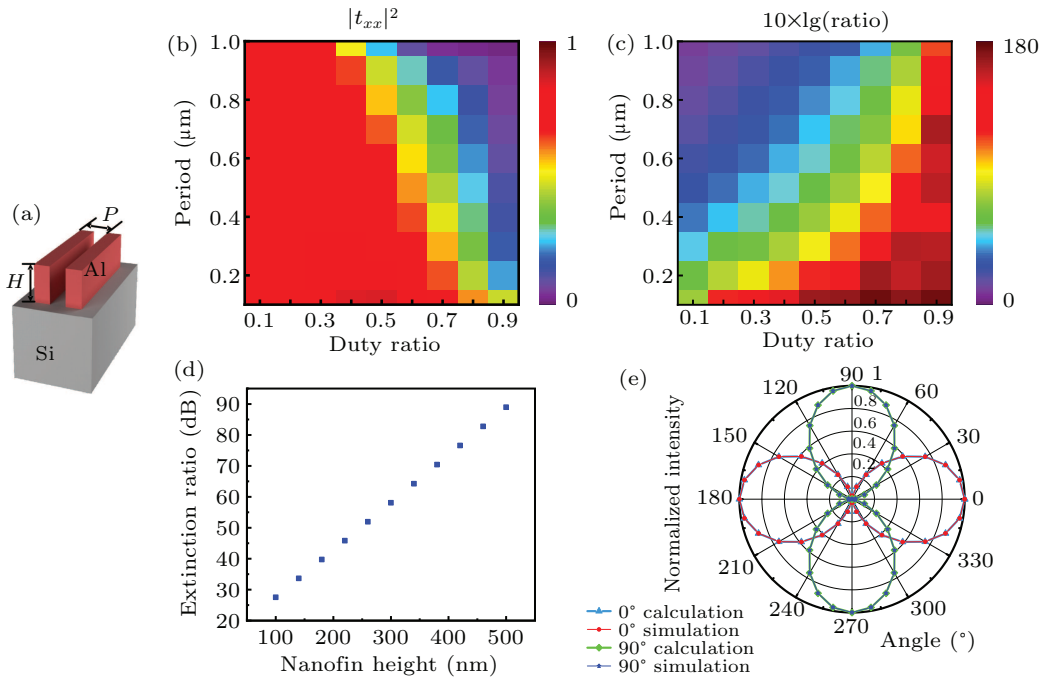


Fig. 2. Simulated intensity and extinction ratio of the transmission coefficients of our designed linear polarized filters. (a) Schematic illustration of an aluminum nanofin positioned on a silicon substrate. The metasurface will comprise a periodic arrangement of such unit cells. (b), (c) Simulation results for the intensity and ratio of the transmission coefficient $|t_{xx}|^2$ and $10\lg(\text{ratio})$ shown for 2D parameter optimization using a rigorous coupled-wave analysis method. The period and duty ratio of the nanofin are swept in the range 0.1–1 μm and 0.1–0.9, respectively, at an incident wavelength of 4.0 μm . (d) Simulation results for the extinction ratio of the linear polarizing filter. The height of the nanofin is swept in the range of 100–500 nm. (e) State of polarization for one spot. The simulated 0° linear polarization is marked by red circles, and the blue dashed line represents the calculated 0° linear polarization. The simulated 90° linear polarization is marked by green circles, and the navy blue dashed line represents the calculated 90° linear polarization.

Thus, the full-Stokes vector of incident light can be calculated. A further real-time polarized image is obtained by calculating the full Stokes vector.

To ensure high performance of the LP filter, such as transmission and extinction ratio, the height, period of the nanofin and duty ratio of the nanofin are optimized. The polarized metasurface is designed using aluminum nanofins on

top of a silicon substrate, as shown in Fig. 2(a). To achieve a high transmittance and large extinction ratio, we perform two-dimensional (2D) parameter optimization using a rigorous coupled-wave analysis method. The period P and duty ratio R of the nanofin are swept in the range of 0.1–1 μm and 0.1–0.9, respectively, while maintaining the height H at 500 nm. The value of H is carefully chosen to guarantee that the extinc-

tion ratio of the polarized metasurface is high. The relationship between the extinction ratio and grating height is shown in Fig. 2(d). The extinction ratio increases with increasing height, but a higher grating height is not conducive to stability and further fabrication.

For the simulation, the nanofin is placed on a silicon substrate ($n_{\text{Si}} = 3.43$). The wavelength of the incident light is fixed at 4000 nm. The obtained transmission amplitudes and extinction coefficients for the two transmission coefficients $|t_{xx}|^2$ and $10 \cdot \lg(\text{ratio})$ are shown in Figs. 2(b) and 2(c). The ratio is equal to $|t_{xx}|^2/|t_{yy}|^2$. It can be found that the transmission coefficient $|t_{xx}|^2$ of the center field of view for the linear polarized filter is over 77% when the height, period and duty ratio are selected as 500 nm, 300 nm and 0.5, respectively. Meanwhile, under the same LP grating geometry, the extinction ratio of the center field of view reaches 88 dB. To demonstrate the high modulation precision, the intensity distribution of the LP components and polarization states is investigated. As shown in Fig. 2(e), the intensity of transmission for the 0° and 90° linear polarized filters is similar to the results of the calculation. Therefore, the designed linear polarizers with four polarization angles can accurately modulate the polarization.

3. Middle-infrared imaging optical system design

To cooperate with the optimized PMMPA element, a real-time MIR polarization optical system for secondary imaging is designed. The basic principle is shown in Fig. 3. To improve the quality of polarization control and reduce the optical energy loss, the objective lens group adopts an image-side telecentric system design. The presented method contains the main rays for each field angle emitted from the object mirror plane that are vertically incident on the PMMPA element.

The intermediate image passing the PMMPA element is imaged on the detector by the relay lens group. To maintain the size of the PMMPA element consistent with the size of the detector, the magnification of the relay system is designed to be 1. Meanwhile, the object-side telecentric system is adopted as the relay lens group.

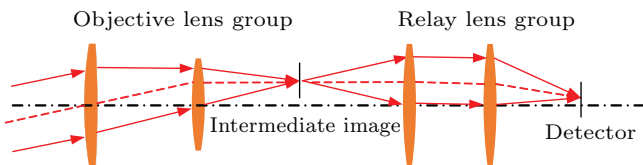


Fig. 3. Basic principle of the real-time MIR polarized optical system for secondary imaging.

According to the imaging principle of the relationship between objects and images

$$\frac{f'}{f} = \frac{l'}{l}. \quad (5)$$

Here f' is the effective focal point of the objective lens group, f is the focal point of the MIR polarized optical system, l' is the height of the PMMPA element and l is the height of the detector. Because l' is equal to l , the focal point of the objective lens system is the focal point of the MIR polarization optical system.

In this design, the image surface of the 12 mm detector is used and the F -number of the detector is 2. The MIR polarized system with a diameter D of 70 mm is designed, and the focal point f of the system is given by

$$F^\# = \frac{f}{D}. \quad (6)$$

Thus, f is equal to 140 mm. The field angle ω of the entire system is given by

$$\omega = \arctan\left(\frac{l}{2f}\right). \quad (7)$$

ω is equal to 5° . Finally, the complete optical design values of the MIR polarization imaging system are shown in Table 1.

Table 1. Values of parameters of the MIR polarized optical imaging system.

Parameter	Value
Wavelength	3.7–4.8 μm
Focal point of MIR system	140 mm
F number of MIR system	2
Focal point of objective lens	140 mm
F number of objective lens	2
Field of view	5°
Magnification	$1\times$

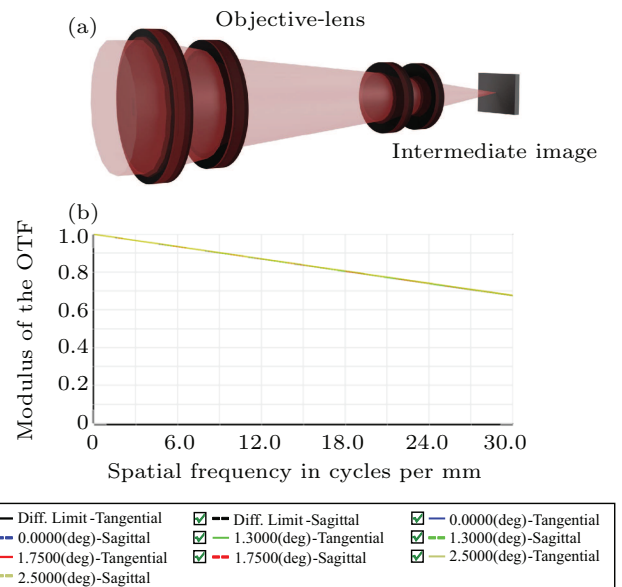


Fig. 4. Result of the MIR objective lens design. (a) Three-dimensional view of the MIR objective lens group. (b) Modulation transfer function (MTF) plots of the MIR objective lens group.

The objective lens and relay lens groups are calculated and optimized, respectively. The power of the system elements and calculation of the initial structure parameters are allocated

according to the primary aberration theory and the presented design theory. After the design, the results of the objective imaging group are shown in Fig. 4(a). Figure 4(b) shows the MTF plots of the objective lens group, which are close to the diffraction limit.

Through calculation of the relationship between the object and image, the magnification of the relay lens group is determined to be 1. An illustration of the final three-dimensional appearance of the MIR relay optical system is shown in Fig. 5(a). As shown in Fig. 5(b), the MTF curve of the relay lens is higher than 0.4 at 33 cycles per micrometer, implying that the performance of the MTF is close to the diffraction limit.

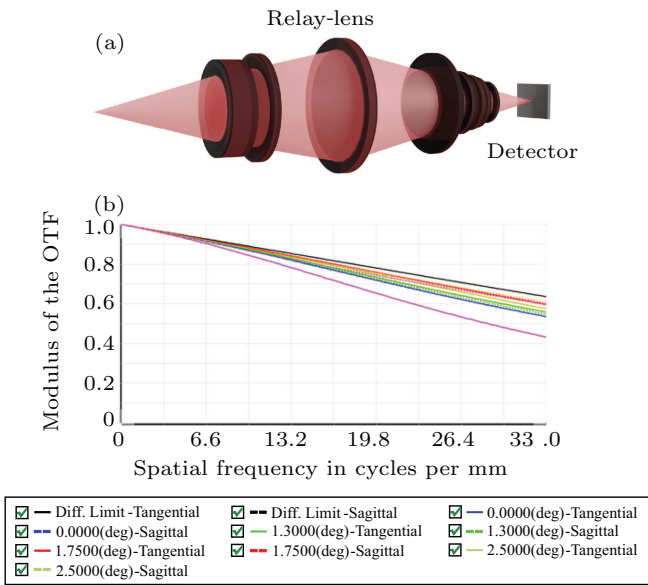


Fig. 5. Result of the MIR relay lens design. (a) Three-dimensional view of the MIR relay lens group. (b) MTF plots of the MIR relay lens group.

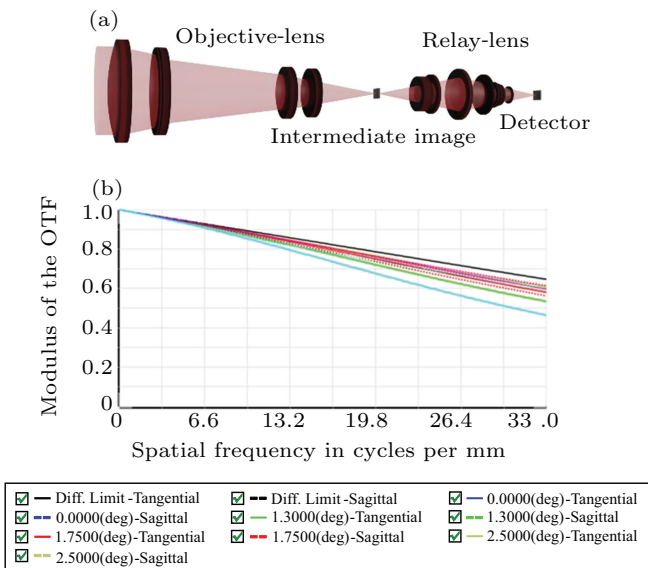


Fig. 6. Result of the whole MIR optical imaging system design. (a) Three-dimensional view of the MIR optical imaging system. (b) MTF plots of the MIR optical imaging system.

When the design of the objective lens group and relay lens system is complete, the objective lens group and relay lens

group are combined into a complete MIR polarization imaging system. After further aberration correction and optical optimization, a real-time MIR optical imaging system is realized. The entire system is illustrated in Fig. 6(a). Figure 6(b) shows the MTF plots of the MIR polarization imaging system, which is close to the diffraction limit at 33 cycles per micrometer. These characteristics satisfy technical requirements.

To realize real-time polarization imaging of the intermediate image plane of the MIR system, the PMMPA element should be designed and placed on the image surface of the objective lens group. Based on the pixel matching theory of a single LP filter and the MIR detector presented in Section 2, the PMMPA element is modeled using optical design software.

The size of a single LP filter is 15 μm. To achieve the four-directional LP filter function, the Jones matrix plane is adopted to represent the LP filters in four polarization directions. The Jones matrix is used to represent the polarization as follows:

$$\begin{pmatrix} \cos^2 \theta & \frac{1}{2} \sin 2\theta \\ \frac{1}{2} \sin 2\theta & \sin^2 \theta \end{pmatrix}, \quad (8)$$

where θ is the angle between the light vector and the x -axis. In this way, the Jones matrices of the four LP filters with polarization angles of 0° , 45° , 90° and 135° are expressed as $\begin{pmatrix} 1 & 0 \\ 0 & 0 \end{pmatrix}$, $\begin{pmatrix} \frac{1}{2} & \frac{1}{2} \\ \frac{1}{2} & \frac{1}{2} \end{pmatrix}$, $\begin{pmatrix} 0 & 0 \\ 0 & 1 \end{pmatrix}$ and $\begin{pmatrix} \frac{1}{2} & -\frac{1}{2} \\ -\frac{1}{2} & \frac{1}{2} \end{pmatrix}$, respectively. These four Jones matrices are arrayed into a polarization element. Partial modeling of the PMMPA element is shown in Fig. 7. The three colored rays represent light incident from different fields of view into different Jones matrix planes. The Jones matrix polarization plane is placed at the middle image plane of the complete MIR imaging optical system. Thereafter, the high transmittance polarization modulation of the outgoing light passing through the PMMPA element is realized.

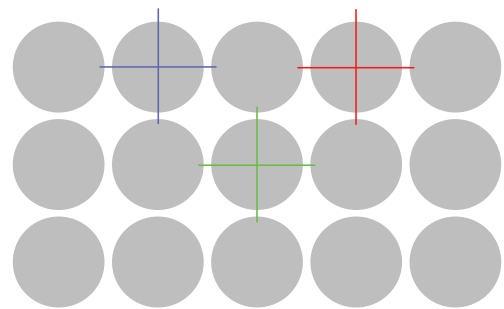


Fig. 7. Partial modeling of the micro-polarization element, which comprises different single Jones matrix type surfaces. The different colored rays represent light incident from several fields of view into different Jones matrix planes.

When the PMMPA element is in the intermediate image plane, efficient transmission of the outgoing light through the device is achieved, and the polarization state of the image surface of the MIR imaging optical system is traced. Figure 8

illustrates the partial results for the different directions of linearly polarized incident light reaching the image plane of the MIR polarization imaging system.

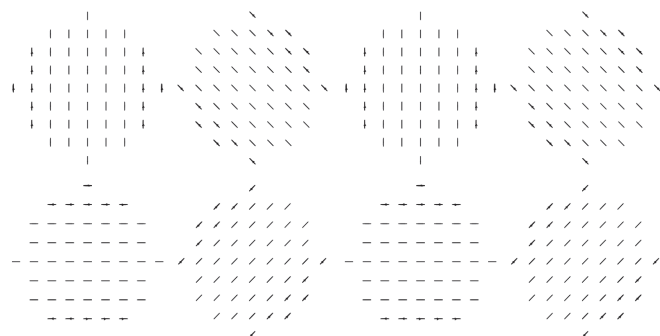


Fig. 8. Partially polarized ray tracing results of the differently polarized light incident on the image plane of the MIR imaging optical system.

According to Fig. 8, the incident light of different fields passing through the PMMPA element and the real-time different directions of polarized intensity images will be obtained by the MIR detector. In the future, the polarization intensity images obtained simultaneously in four polarization directions on the image plane will be processed. A single pixel corresponds to an intensity image in the LP direction, which is conducive to image registration and real-time polarization imaging of the target within the field of view.

4. Conclusion

A method using a pixel-matched micro-polarization array on the middle image plane of the MIR imaging system to realize real-time polarization imaging is presented. This method can achieve the same function as real-time polarization imaging as DOFP. The PMMPA element based on the metasurface comprises multiple different polarization angle LP filters. Simultaneously the geometrical size of the microstructure on the surface of the PMMPA element is optimized. The LP filters can well transmit the linear polarization of the emergent light with the transmission of the center field of view as high as 77% at 4.0 μm when the H is 500 nm, P is 300 nm, R is 0.5, and the extinction ratio of the center field of view is 88 dB. On this basis, an MIR polarization imaging optical system near the diffraction limit with a FOV of 5° , a focal length of 140 mm, and an F -number of 2 is designed. A micro-polarization array comprising the Jones matrix plane is arranged in the intermediate image plane to analyze the performance of the polarized imaging. The simulation results show that the emergent light from the PMMPA element can achieve real-time polarized imaging in different polarization directions on the image

plane. This method provides a new approach for the realization of MIR real-time polarization imaging.

Acknowledgement

Project supported by the National Key R&D Program of China (Grant No. SKLA02020001A05).

References

- [1] Jin L W, Claborn K A, Kurimoto M, Geday M A, Maezawa I, Sohraby F, Estrada M, Kaminsky W and Kahr B 2003 *Proc. Natl. Acad. Sci. USA* **100** 15294
- [2] Cui X Y, Nichols S M, Arteaga O, Freudenthal J, Paula F and Shtukenberg A G 2016 *Am. Chem. Soc.* **138** 12211
- [3] Zhao H J, Li Y S, Jia G R, Li N, Ji Z and Gu J R 2018 *Appl. Opt.* **57** 6840
- [4] Tyo J S, Goldstein D H, Chenault D B and Shaw J A 2006 *Appl. Opt.* **45** 5451
- [5] Tyo J S, Goldstein D L, Chenault D B and Shaw J A 2006 *Appl. Opt.* **45** 5453
- [6] Li S J, Jiang H L, Zhu J P, Duan J, Fu Q, Fu Y G and Dong K Y 2013 *Chin. Opt.* **6** 803
- [7] Maruyama Y, Terada T, Yamazaki T, Uesaka Y and Ezaki T 2018 *IEEE Trans. Electron Devices* **65** 2544
- [8] Zhang J, Luo H, Hui B and Chang Z 2016 *Opt. Express* **24** 20799
- [9] Harnett C K and Craighead H G 2002 *Appl. Opt.* **41** 1291
- [10] Tyo J S 2006 *Opt. Lett.* **31** 2984
- [11] Liu X, Chang J, Zhong Y, Feng S, Song D L and Hu Y Y 2020 *J. Mod. Opt.* **67** 462
- [12] Gruev V, Perkins R and York T 2010 *Opt. Express* **18** 19087
- [13] Gruev V, Ortu A, Lazarus N, Van der Spiegel J and Engheta N 2007 *Opt. Express* **15** 4994
- [14] Zhao H J, Li Y S, Jia G R, Li N, Ji Z and Gu J R 2018 *Appl. Opt.* **57** 6840
- [15] Liu X, Chang J, Feng S, Mu, Y, Wang X and Xu Z P 2019 *Chin. Phys. B* **28** 084201
- [16] Zhao Y Q, Zhang L, Zhang D and Pan Q 2009 *Comput. Vis. Image Underst.* **113** 855
- [17] Yang Z Y, Zhao M, Lu P X and Lu Y F 2010 *Opt. Lett.* **35** 2588
- [18] Frank B, Yin X, Schäferling M, Zhao J, Hein S M, Braun P V and Giessen H 2013 *ACS Nano* **7** 6321
- [19] Zhang M, Pacheco-Peña V, Yu Y, Chen W, Greybush N J, Stein A, Engheta N, Murray C B and Kagan C R 2018 *Nano Lett.* **18** 7389
- [20] Gansel J K, Thiel M, Rill M S, Decker M, Bade K, Saile V, Freymann G, Linden S and Wegener M 2009 *Science* **325** 1513
- [21] Decker M, Klein M W, Wegener M and Linden S 2007 *Opt. Lett.* **32** 856
- [22] Kwon D H, Werner P L and Werner D H 2008 *Opt. Express* **16** 11802
- [23] Afshinmanesh F, White J S, Cai W and Brongersma M L 2012 *Nanophotonics* **1** 125
- [24] Ye W, Yuan X, Guo C, Zhang J, Yang B and Zhang S 2017 *Phys. Rev. Appl.* **7** 054003
- [25] Chen W, Abeyinghe D C, Nelson R L and Zhan Q W 2010 *Nano Lett.* **10** 2075
- [26] Rubin N A, Aversa G D, Chevalier P and Capasso F 2019 *Science* **365** eaax1839
- [27] Chen C, Wang Y, Jiang M W, Wang J, Guan J, Zhang B S, Wang L, Lin J and Jin P 2020 *Nano Lett.* **20** 5428
- [28] Yao Z and Chen Y H 2021 *Opt. Express* **29** 3904